Wind impacts on suspended sediment transport in the largest freshwater lake of China

Hua Wang, John Paul Kaisam, Dongfang Liang, Yanqing Deng and Yuhan Shen

ABSTRACT

Poyang Lake, the largest freshwater lake in China, is distinguished by complicated suspended sediment (SS) dynamics. Apart from lake currents, wind is an important form of natural disturbance in driving SS transport. Combining field data, laboratory experiments, and numerical simulations, we gained valuable insight into wind impacts on SS dynamics in Poyang Lake. (1) Lake current patterns exert great influence on the level of wind impacts. Due to reduced sediment carrying capacity, SS under weak current suffers from stronger wind influence than under strong currents. (2) Wind speed determines the degree of wind impact, not only affecting horizontal SS transport, but also regulating vertical dynamics. Winds exceeding critical intensity can enhance horizontal transport through both surface drift and Stokes drift at different water depths, triggering sediment suspension to feed the loads in overlying water. (3) Wind impact is influenced by lake morphology. The broad water surface in the central lake permits formation of continuous waves, leading to the largest SS fluctuation, from $-10.05\ mg{\cdot}L^{-1}$ to $+20.17\ mg{\cdot}L^{-1}$, while average variation in the south and north part of the lake is only $-6.59\ mg{\cdot}L^{-1}$ to $+10.36\ mg{\cdot}L^{-1}$. (4) SS in four reserves are characterized by notable wind impact, while in the other two reserves SS show no obvious departure from values without wind.

Key words | numerical experiment, Poyang Lake, shear stress, suspended sediment, wind

Hua Wang (corresponding author)
John Paul Kaisam
Yuhan Shen
Key Laboratory of Integrated Regulation and Resource Development on Shallow Lake of Ministry of Education, College of Environment,
Hohai University,
Nanjing 210098,
China
and
College of Environment,
Hohai University,
Nanjing 210098,
China
E-mail: *wanghua543543@163.com*

John Paul Kaisam
Department of Chemistry, School of Environmental Sciences,
Njala University,
Bo City,
Sierra Leone

Dongfang Liang
Department of Engineering,
University of Cambridge,
Cambridge CB2 1PZ,
UK

Yanqing Deng
Hydrology Bureau of Jiangxi Province,
Nanchang 330002,
China

HIGHLIGHTS

- Current patterns have varied consequences for wind-driven impacts on SS transport.
- Wind regulates both horizontal and vertical dynamics of SS.
- Wind-driven impact has a relationship with lake morphologies.
- SS distribution in Poyang Lake closely interacts with wind events.

INTRODUCTION

Suspended sediment (SS) is an important member of the water environment system (Westall 2005; Horowitz 2008). The transport of SS has a wide variety of consequences in natural and artificial water bodies (Edmonds & Slingerland 2010; Constantine *et al.* 2014). First, SS contributes to the morphodynamic changes of water boundaries and bottom topographies, which may exert negative effects on flood control, irrigation, power generation, shipping, aquaculture, and water landscape. The over-supply of sediment may also result in aggradation that cover the habitats of aquatic animals and cause a decrease in the function of stream installations. A sediment under-supply causes the degradation of the river bed, which can endanger stream installations such as banks and bridge piers by undermining

doi: 10.2166/nh.2020.153

their foundations (Poff *et al.* 1997). Moreover, SS always acts as a carrier of pollutants and alters the chemical and biological properties of the aquatic environment (Hossain *et al.* 2004). It participates in the vertical transport of pollutants between overlying water and surface deposited sediment, as well as the horizontal migration; for example, heavy metal adsorbed onto SS in the upstream will aggravate the pollution load in estuaries (Yin *et al.* 2016). Sediment suspension-induced nutrient release may accelerate harmful cyanobacterial blooms in a shallow freshwater lake (Qiu *et al.* 2016).

The dynamics of SS in water are related to the combination of many factors, such as particle characteristics, water current, and plant resistance. Current intensity is recognized as the dominant force driving SS transport, and decades of research have yielded insight into this point. Jane *et al.* (1987) investigated the transported SS in Lake Houston, US and found that the circulation in the lake was periodically intense enough to transport coarse silt in suspension. Hawley *et al.* (2009) disclosed the transport mechanisms of SS in Lake Michigan, US by numerical simulation. Zhong *et al.* (2014) determined the drift velocity of SS in turbulent open channel flows based on the Favre-averaged two-fluid equations. These studies laid an important foundation to illuminate the movement mechanism of SS in water bodies. However, few studies have addressed factors beyond wind impact as a contributor. Among the main studies of wind's influence on SS transport are those of Sheng & Lick (1979), Thomas & Takhar (1992), and Constantin (2006), who identified that wind could play a major role in sediment transport in various forms. Below a critical wind speed, SS in the upper water volume are apt to flow toward the downwind axis, while under the stronger wind speed, the generated turbulence can not only enhance the lateral SS transport but also be capable of resulting in spontaneous resuspension events which may increase the total SS load in overlying water. Furthermore, especially in the case of strong and long duration winds, besides the surface transport, SS distributed in deeper layers can still be driven by the wind-generated stokes drift which interacts with, and often contributes to, lateral SS transport (Stokes 1847). These researchers made efforts to explore the wind's impacts on sediment transport; however, most of the documented results remained at the level of qualitative description, and limited work was directed to probing the difficulties in quantitative determination. As wind generally affects a relatively limited area and is infrequent at a specific site, its impacts may not be as significant in lakes or rivers compared to more regular current forces. However, SS transport during different wind events may also have critical impacts on ecosystem functioning by modifying sediment delivery to nearby marshes (Perez *et al.* 2000; Draut *et al.* 2005), nutrient transport, and other biogeochemical fluxes both within, and out of, the system (Day *et al.* 2000; Carlin *et al.* 2016). Thus, a better understanding of wind impacts on SS transport is essential for a better understanding of many eco-environment processes.

Poyang Lake is the largest freshwater lake in China, as well as the most typical river-connected lake in the world's top 50 freshwater lakes (Figure 1). Unlike isolated lakes such as Lake Taihu, China and Lake Tana, Ethiopia, Poyang Lake gathers water runoff from five upstream rivers and then feeds the Yangtze River at Hukou through a northern channel (Mekete *et al.* 2015; Wang *et al.* 2016). SS in the lake is distinguished by a notable spatial-temporal distribution. In addition, Poyang Lake is one of the world's six largest wetlands in the Ramsar Convention List recognized by the Global Natural Fund. It is an ecological treasury with global significance (Ji *et al.* 2012; Zhang *et al.* 2012; Han *et al.* 2015). It provides the world's largest overwintering area for more than 95% of the world's white cranes, and provides important places for finless porpoises for feeding, nurture, and play. Both of these two species were identified as 'Critically Endangered A3b + 4b' on the red list of International Union for Conservation of Nature (IUCN) (Su *et al.* 2000; Zhao *et al.* 2012). The complicated process of SS in Poyang Lake may change the distribution of varied pollutants including nutrients, heavy metals, organic contaminants, and nano-pollutants, which may exert direct or indirect health risks on the sensitive species. A better study on SS dynamics can yield better insight into pollutant migration. Currently, some researchers are paying attention to SS transport in Poyang Lake, but most of them have focused on the runoff-induced dynamic conditions (Cui *et al.* 2013; Gao *et al.* 2014; Zhang *et al.* 2016). Little information is available concerning the wind impacts on SS transport in the lake. As Poyang Lake is located in the monsoon region, wind is an important factor influencing SS

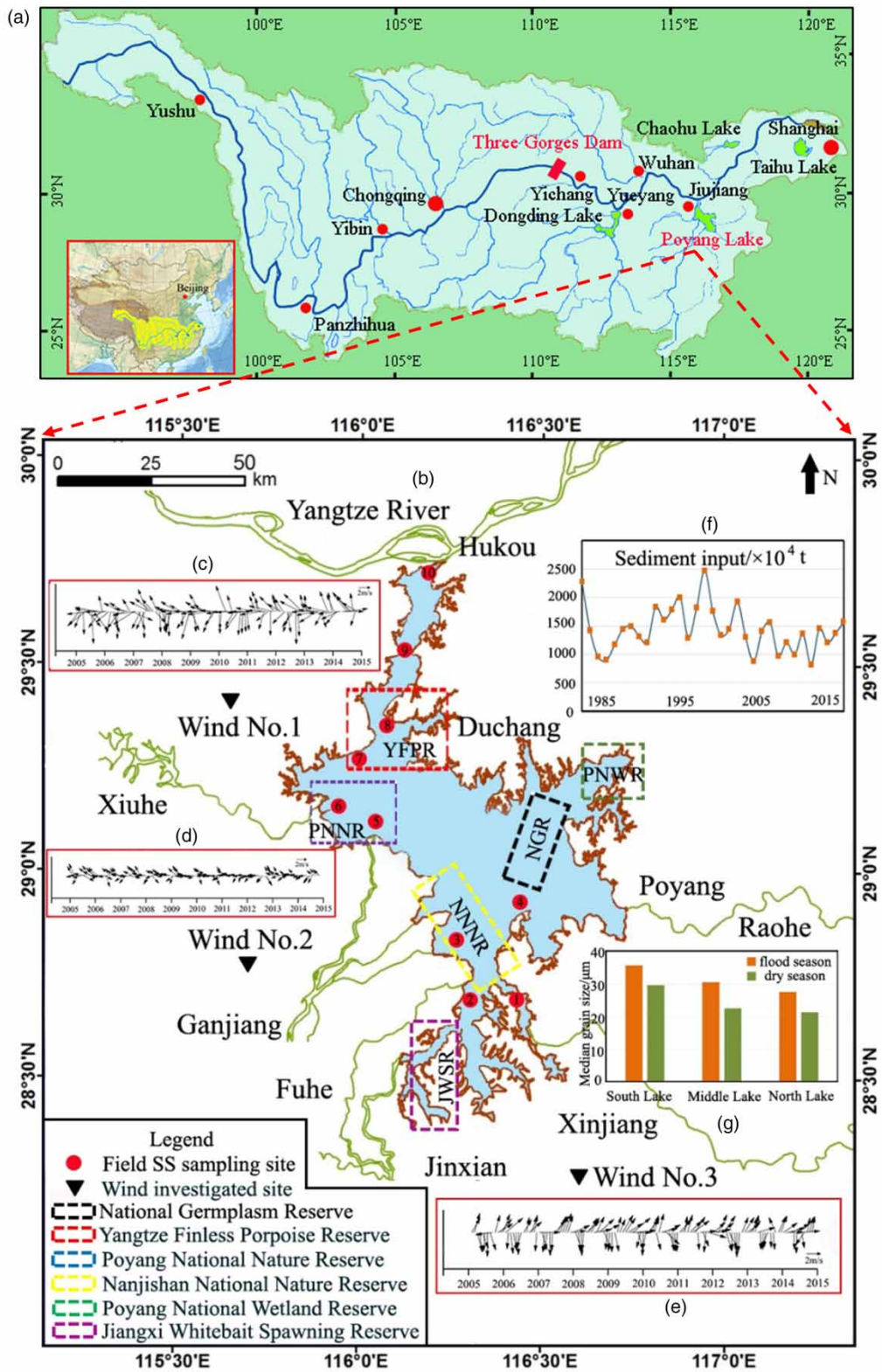

Figure 1 | (a) Location of Poyang Lake in the Yangtze River Basin and China. (b) Map of Poyang Lake. Locations of ecological reserves and field investigation sites are indicated. Inserts (c), (d), and (e), respectively, represent the wind distribution in the north, central, and south lake. (f) The processes of sediment input into Poyang Lake from 1983 to 2016. (g) Grain-size variation in the lake.

transport. In the present work, we place the emphasis on wind impacts on SS transport in Poyang Lake. The objectives were to: (1) investigate the suspension mechanism associated with varied grain-size sediments, triggered by different shear stresses from the surface deposited sediment; (2) develop and validate an improved SS transport model that incorporates the contribution of surface transport and Stokes drift induced by different wind events; (3) use numerical experiments to quantitatively reveal the spatial SS distribution under the combination of varied currents, gravity-pattern, jacking-pattern, and backflow-pattern, and different wind events, light wind ($0.3\ m{\cdot}s^{-1}$–$1.6\ m{\cdot}s^{-1}$), gentle wind ($3.4\ m{\cdot}s^{-1}$–$5.5\ m{\cdot}s^{-1}$), moderate wind ($5.5\ m{\cdot}s^{-1}$–$8.0\ m{\cdot}s^{-1}$), hard wind ($8.0\ m{\cdot}s^{-1}$–$10.8\ m{\cdot}s^{-1}$), and strong wind ($10.8\ m{\cdot}s^{-1}$–$13.9\ m{\cdot}s^{-1}$); (4) evaluate the influences of wind events on SS dynamics in the lake, especially the regions related to the critically endangered white cranes and finless porpoises.

MATERIALS AND METHODS

Study area

Poyang Lake, with an area of 3,583 km^2 and a volume of 27.6 km^3, on average, is located on the south bank of the Yangtze River in Jiangxi Province, China (Wu *et al.* 2007). It is a typical river-connected lake. When the water level at Hukou station increased from its lowest 5.9 m (observed on February 6, 1963) to its highest 22.59 m (observed on July 31, 1998), the mean water depth increased from 4.5 m to 6.8 m. The lake, which hosts millions of birds (over 300 species) (Lu *et al.* 2012; Han *et al.* 2015; You *et al.* 2015), exerts important roles in flood-mitigation storage, regulation of the local climate, and as protection of global biodiversity. The lake receives water from five rivers (Raohe, Xinjiang, Fuhe, Ganjiang, and Xiuhe) and drains into the Yangtze River through a narrow outlet to the north (Feng *et al.* 2013). Due to the river–lake interaction, the area and volume of Poyang Lake vary considerably throughout the year (Liu & Rossiter 2008; Volpe *et al.* 2011). It expands to a large water surface during the wet season, but shrinks to little more than a river during the dry season. Poyang Lake is characterized by marked intra- and inter-annual variations of suspended sediment load (Wang *et al.* 2014, 2015). According to the measured data from 1956 to 2015, the mean concentration of SS load in Poyang Lake is approximately $0.120\ kg{\cdot}m^{-3}$, with the peak and valley values being $0.185\ kg{\cdot}m^{-3}$ and $0.036\ kg{\cdot}m^{-3}$, respectively (Cui *et al.* 2013; Wang *et al.* 2015). Sediment in the lake derives from varied pathways including the five upstream rivers, backflow water from the Yangtze River, blown sand, and bank caving. The upstream inflowing rivers mainly contribute 87.2% of the total load (Yarnell *et al.* 2006; Cheng *et al.* 2013). The sediment load entering Poyang Lake greatly changed due to human activities, especially land cover changes such as the aggravating deforestation induced by anthropogenic activities. The forest coverage in the lake watershed decreased from 40.1% in 1950 to 31.5% in the early 1980s, leading to serious soil erosion. In recent years, the mean volume of transported SS from Gan, Fu, Xin, Rao, and Xiu rivers to the lake in a year could reach 9.16×10^6 t, 2.12×10^6 t, 1.43×10^6 t, 0.99×10^6 t, and 0.80×10^6 t, respectively (Xiong 1990). The lake basin has a subtropical monsoon climate, with an average annual temperature of 18 °C, precipitation of 1,636 mm, and evaporation of 1,044 mm during 1953–2002 (Guo *et al.* 2008). Due to the Siberia cold air current, the north wind is characterized by the highest frequency of 56% in winter and spring. Attributed to the control of Pacific Subtropical High, the south wind is the second prevailing one, especially in summer and autumn, of which the occurrence frequency is about 30%. According to the data of 1964–2005, the annual mean wind speed on Poyang Lake was approximately $3.8\ m{\cdot}s^{-1}$ and the periods when daily mean wind speed $\geq 5\ m{\cdot}s^{-1}$ could reach 99.4 d/year (Cao *et al.* 2015). The maximum wind intensity is $31\ m{\cdot}s^{-1}$, monitored at Tangyin station on April 8, 1982. Investigation of the wind-induced impacts on SS transport is of great significance to explore water quality variation, bio-geochemical cycling, and eco-environment evolution in Poyang Lake.

Data acquisition and processing

Data for the simulation experiments were collected from various sources. The boundary data for the five upstream rivers, including water quantity and suspended sediment,

were determined according to the measured data acquired from the Jiangxi Province Hydrology Bureau. Hydrology and suspended sediment data of the Yangtze River were obtained from the 'Hydrological Yearbook of the Yangtze River Basin, China'. Information needed to establish model geometry was determined from a remote sensing image acquired on October 5, 2007 (Lei *et al.* 2010). Lake bottom data were derived from the 2010 survey, in which 439 pieces of 1:10,000 DEM data were established to describe the whole lake area. Suspended sediment classification was refined by referring to the irregular field observations at the inlet areas of Raohe, Xinjiang, Fuhe, Ganjiang, and Xiuhe, with the help of the Poyang Lake Hydrology Bureau. Water current data obtained from the field investigations of 2010 (October 9–12, December 19–20, and December 28–29), were used in conjunction with the data collected on May 17–18, 2012 to aid model calibration and validation. The suspended sediment data utilized for model test were collected from the 19 regular investigated points covering the entire lake. The variation in wind data for the studied year 2010 was discretized into five classes for each month, with their associated frequencies of occurrence, on the basis of the continuous wind data obtained from the online database of the China National Meteorological Information Center.

Laboratory experiment

Wind can disturb the turbulent diffusion of SS, as well as enhance the bed shear stress, which promotes SS exchange between the surface deposited sediment and overlying water. How wind triggers sediment suspension is dominated by the combination of wind events, water depth, and the grain diameter of sediments. As little attention has been paid to the relationships between bottom shear stress and the dynamics of sediments with different diameters in Poyang Lake, we conducted flume experiments to provide a quantitative insight into the suspension mechanisms of sediments with different sizes. Based on field investigation, the lake is marked by a prevalence of SS in the range of 8.0 μm–78.0 μm, and three sediment size classes, fine-silt (3.79–16.8 μm), medium-silt (16.8–32.57 μm), and coarse-silt (32.57–63.0 μm), were arranged to explore the starting rules. The important variable in the experiment was the bottom shear stress, which can be applied to field conditions under different current patterns and wind events. The flume experiments here were conducted to provide a quantitative insight into the suspension mechanisms of sediments with different sizes. The results will contribute to optimizing the parameter of source-sink vector of SS in the following numerical model, and therefore improve its performance. The experiment was carried out in the Molecular Biology Laboratory of Nanjing Geography and Limnology Institute, Chinese Academy of Sciences in August to September, 2014.

The annular flume, which is composed of flume and top lid, was applied to generate continuous currents (Figure 2). The flume and top lid are made of acrylic material with outer diameter of 120 cm and inner diameter of 80 cm. The annular water channel is 20 cm in width and 41 cm in depth, and the top lid can go up and down to maintain the water depth. Sample outlets were set at different heights on the external wall of the flume. The flume and top lid could rotate independently by control of the computer system. Driven by different motors, the rotation of the flume and top lid in opposite directions can create the water currents. Given that the centrifugal force is related to rotation rate, the secondary flows produced by rotation could be avoided by adjusting the rotation rates of the top lid and flume to form a homogeneous water current (Wang *et al.* 2017). Prior to the experiment, sawdust was selected as a tracer indicator to calibrate the device. According to the *in situ* flow velocity in Poyang Lake, the currents in the flume were set at six grades including 0 $m \cdot s^{-1}$, 0.1 $m \cdot s^{-1}$, 0.2 $m \cdot s^{-1}$, 0.3 $m \cdot s^{-1}$, 0.5 $m \cdot s^{-1}$, and 0.7 $m \cdot s^{-1}$. After the change of rotational speeds, 30 minutes of waiting time was introduced to form a stable flow. The sediment was stirred and spread evenly at the bottom of the flume, and after 1 day's deposition, the overlying water was slowly poured into the test depth 24 cm to start the experiment. Three groups of disturbance experiments were arranged separately for fine-, medium-, and coarse-silt. SS concentration was determined by gravimetric method during the experiment.

Generally, the incipient motion of sediment can be divided into the following three levels, individual movement, ounce movement, and universal movement (Xiao

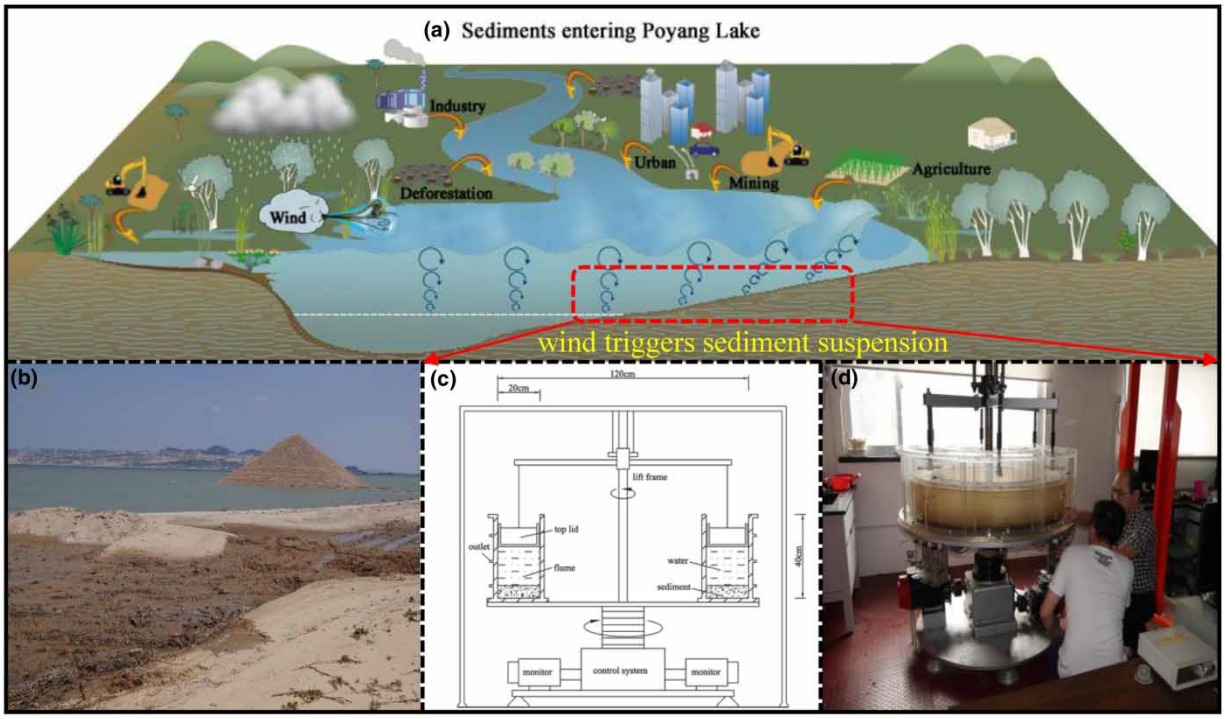

Figure 2 | (a) The wind impacts in both vertical and horizontal direction. (b) A live picture exhibiting the field sediment on the lakeshore. (c) Schematic diagram of the experimental device and primary equipment are indicated. (d) A live picture of the dynamic experiment.

et al. 2009). To place the emphasis on wind impacts, individual movement with the suspension rate of 1% was fixed to determine the sediment starting criterion in the present work. Moreover, the starting velocity can be used as an index to reflect sediment incipient motion, but it is not convenient in popularization and application (Yang & Wang 1995; Pang *et al.* 2012). Thus, the depth-averaged velocity in the flume was transferred into bed shear stress by the following equations which are written as follows:

$$\begin{cases} \tau_e = \rho \cdot u_*^2 \\ \dfrac{u_c}{u_*} = \dfrac{1}{\kappa} \ln \dfrac{h_c}{k_s} + B_s \end{cases} \quad (1)$$

where τ_e is the critical sediment starting shear stress, ρ is water density, u_* is the friction velocity, u_c is the section-averaged flow velocity, κ is Karman constant, h_c is 0.37 times of the water depth to the bed surface (Chao *et al.* 2008; Li 2008), k_s is sand roughness taken as sediment diameter, B_s is the dimensionless parameter of the water flow near the bed surface.

Numerical model establishment

A 2-D model was built to yield accurate simulations of SS transport in Poyang Lake under the combination of wind and currents. To compute the effects of particle size variation, three sediment size classes, fine-silt (3.79–16.8 μm), medium-silt (16.8–32.57 μm), and coarse-silt (32.57–63.0 μm), were simulated in the present study. Poyang Lake can be assumed to be vertically well mixed, and the general three-dimensional equations were allowed to be approximated by two-dimensional, vertically integrated equations on the basis of the following facts. First, the huge water surface of 3,583 km^2 enlarges the mean width–depth ratio to 1.52×10^4, which is calculated by the mean horizontal scale and the mean water depth. The high ratio prefers 2-D simulation. Second, the intense river–lake relationship diminishes the water exchange period to 6.8 d–22 d in the lake, which hinders stratification. 2-D simulation can avoid the large computational workload and improve the simulation efficiency. Third, Poyang Lake is marked by a prevalence of SS in the range of

8.0 μm–78.0 μm that belongs to the grade of silt sand. The concentration of SS in the vertical distribution did not exhibit evident difference to the lakes which were characterized by wider SS range and higher water depth. Based on the Navier–Stokes equation, a 2-D water current–sediment coupled model was established, in which the wind stress was embedded as well as the inertial force, Coriolis force, and viscous force. The conservation forms of water flow and suspended sediment transportation can be expressed as follows (Periáñez 2009; Pu *et al.* 2012; Pu 2015):

$$\begin{cases} \dfrac{\partial \delta}{\partial t}+\dfrac{\partial (h+\delta)u}{\partial x}+\dfrac{\partial (h+\delta)v}{\partial y}=0 \\ \dfrac{\partial u}{\partial t}+u\dfrac{\partial u}{\partial x}+v\dfrac{\partial u}{\partial y}=-g\dfrac{\partial \delta}{\partial x}+\varepsilon\nabla^2 u+F_x+fv \\ \dfrac{\partial v}{\partial t}+u\dfrac{\partial v}{\partial x}+v\dfrac{\partial v}{\partial y}=-g\dfrac{\partial \delta}{\partial y}+\varepsilon\nabla^2 v+F_y-fu \\ \dfrac{\partial (hS_i)}{\partial t}+\dfrac{\partial (huS_i)}{\partial x}+\dfrac{\partial (hvS_i)}{\partial y}=\dfrac{\partial}{\partial x}\left(\lambda D_{xi}h\dfrac{\partial (S_i)}{\partial x}\right) \\ \qquad +\dfrac{\partial}{\partial y}\left(\lambda D_{yi}h\dfrac{\partial (S_i)}{\partial y}\right)+F_s,\ i=1,2,3 \end{cases} \tag{2}$$

where h is water depth, t is time, u and v are the depth-averaged velocity components in x and y directions, g is the acceleration of gravity, δ is the difference between water surface elevation and the average elevation. ε is the eddy viscosity coefficient, f is the Coriolis force parameter, S_i is the suspended sediment concentration associated with the i-class sediment (i = 1, 2, 3, respectively, representing fine-silt of 3.79 μm–16.8 μm, medium-silt of 16.8 μm–32.57 μm, and coarse-silt of 32.57 μm–63.0 μm); D_{xi} and D_{yi} are the dispersion coefficients of i-class suspended sediment in the x and y directions; F_s is the source-sink vector of SS, which is the net flux of suspension and deposition. F_x and F_y are the friction force in x and y directions. F_x, F_y, f, and F_s can be expressed as follows (Snorri *et al.* 2004):

$$\begin{cases} F_x=\dfrac{\tau_{wx}-\tau_{bx}}{\rho\omega(h+\delta)},\ F_y=\dfrac{\tau_{wy}-\tau_{by}}{\rho\omega(h+\delta)} \\ F_s=-A\varpi S(1-\dfrac{\tau}{\tau_d})+BM(\dfrac{\tau}{\tau_e}-1), \\ A=\begin{cases}1, \tau\le\tau_d \\ 0, \tau>\tau_d\end{cases},\ B=\begin{cases}1, \tau\ge\tau_e \\ 0, \tau<\tau_e\end{cases} \\ f=2\omega\sin\varphi \end{cases} \tag{3}$$

where τ_{wx} and τ_{wy} are, respectively, the wind stress velocity components in x and y directions, τ_{bx} and τ_{by} are the friction force components of lake bottom. ρ is the water density, ω is the earth's rotation angular velocity, M is the scouring coefficient, ϖ is the deposition velocity of sediment, τ is the shear stress at the deposit sediment surface, τ_d is the critical deposition shear stress, τ_e is the critical starting shear stress. When $\tau \ge \tau_e$, the deposited sediment starts to suspend, and the bottom bed is scoured. When $\tau \le \tau_e$, the suspended sediment began to settle, and sedimentation was exerted on the bottom bed. τ_d is usually a bit less than τ_e, and here, to simplify calculation, the two shear stresses were approximately recognized as the same. It was considered that the flow velocity at the balanced status (non-deposition and non-eroding) was not a range (from the critical deposition velocity to the critical starting velocity) but a point (the critical starting velocity). φ is the latitude of research area. The calculation of wind stress, lake bottom friction force, and the shear stress on the deposit sediment surface can be written as follows (Choi & Lee 2015; Carlin *et al.* 2016; Pu 2019):

$$\begin{cases} \tau_{wx}=\dfrac{\rho_a}{\rho}\alpha U_x\sqrt{U_x^2+U_y^2} \\ \tau_{wy}=\dfrac{\rho_a}{\rho}\alpha U_y\sqrt{U_x^2+U_y^2} \\ \tau_{bx}=\dfrac{gu\sqrt{u^2+v^2}}{c^2h},\ c=h^{1/6}/n \\ \tau_{by}=\dfrac{gv\sqrt{u^2+v^2}}{c^2h},\ c=h^{1/6}/n \\ \tau=(\tau_c+\tau_w\sin\theta)^2 \end{cases} \tag{4}$$

where ρ_a is air density, taken as 1.02 kg·m^{-3}; U_x and U_y are, respectively, the wind speed components in x and y directions 10 m from water surface; α is the wave stress coefficient, which is related to the wave-particle amplitude; c is the Chezy coefficient; n is the Manning coefficient; τ_c is the shear stress of lake bed; τ_w is the shear stress of lake bed under wind force; θ is the argument. λ is the correction coefficient of wind on physical *SS* transportation, which can be calculated by Equation (5). Here, we established a piecewise function between wind speed and correction coefficient. Under the winds having high speeds, the surface deposited sediments are mixed to the overlying water and the wave-generated stokes drift was incorporated to optimize the dynamics of SS. Stokes drift is an important vector component that appears often in wave averaging.

An obvious difference between the Stokes wave and the micro-amplitude wave is that the water quality point does not have a closed track. After a period of water point movement, there is a net horizontal displacement. This net horizontal displacement results in a horizontal flow and mass transport:

$$\lambda = \begin{cases} 1, u_w = 0 \\ 1 + u_{sd}/\sqrt{u^2 + v^2}, 0 < u_w \le u_c \\ 1 + u_{st}/\sqrt{u^2 + v^2}, u_w > u_c \end{cases} \quad (5)$$

where, u_w is the wind speed; u_{sd} is the wind-induced surface drift velocity; u_{st} is the Stokes drift velocity; u_c is a critical wind speed. In view of the finite depth in Lake Poyang, u_{sd} and u_{st} are calculated by the following formula (Jan 1982; Dag 2015; Ran *et al.* 2015):

$$u_{sd} = u_w\sqrt{\rho_a \eta/\rho}, u_{st} = \frac{\pi^2 H^2}{L^2} c \frac{\cosh(kh)}{\sinh^2(kh)} \quad (6)$$

where, ρ_a is the density of air; η is the wind drag coefficient; H is wave height; L is wave length; c is wave velocity; k is wave number, 2π/L. On the basis of *in situ* observations of wind waves on the surface of Poyang Lake, the wave parameters are all determined by the method of Sverdrup-Munk-Bretschneider. The coefficient η determines the momentum transfer rate between atmosphere and lake. It varies with the wind speed and is related to the surface roughness. In the present work, it was initially evaluated according to the following empirical formula. We have supplemented the related information.

$$\eta = (0.75 + 0.067U_{10}) \times 10^{-3} \quad (7)$$

where, U_{10} is the wind speed at 10 m elevation.

During simulation, the water flow and SS transport equations were combined to be resolved. For any element, the equations were solved in the framework of finite volume method and the normal fluxes of the variables across the interfaces between elements were calculated by the flux vector splitting scheme. This scheme is based on characteristic theory. It accords with fluctuation view, and reflects the upwind principle. By splitting flux difference on any interval, the numerical flux across the unit boundary can be resolved.

Numerical simulation schemes

Water currents in Poyang Lake are strongly influenced by the combined impacts of the five upstream rivers and the Yangtze River downstream. Given the temporal gap between the flood peaks of the upstream and downstream rivers, currents in Poyang Lake can be divided into the following three types. (1) Gravity-pattern current, the primary current type. Water flows from south to north, in accordance with the main channel, and the flow velocity is mainly driven by the water surface slope. (2) Jacking-pattern current, the second dominant current. It is a transitional current between gravity- and backflow-pattern current. Here, 'jacking' means Poyang Lake can receive water from five rivers (Gan River, Fu River, Xin River, Rao River, and Xiu River) but cannot drain into the Yangtze River, normally due to the high-water level. This kind of current is formed from April to August when water levels in the five upstream rivers and the downstream Yangtze River rise at the same time, or at the end of the flood season of the five upstream rivers, during which the water level of the downstream Yangtze River is still rising. Under this kind of current, the flow velocity in the whole lake is evidently decreased. (3) Backflow-pattern current, mainly observed between July and September. This kind of current is induced by the flood of the Yangtze River. It always happens when the flood season of the five upstream rivers is finished and the water level in the Yangtze River is higher than the lake water level. The numerical experiments were determined upon the consideration of both currents and wind events. Under a given current pattern, varied wind intensities in the prevailing direction were incorporated. Due to the vast lake surface, wind events always show obvious departure among the north, central, and south lakes. To simplify calculation, the daily maximum wind intensity was recognized to separate the wind grades, including light wind (0.3 $m{\cdot}s^{-1}$–1.6 $m{\cdot}s^{-1}$), gentle wind (3.4 $m{\cdot}s^{-1}$–5.5 $m{\cdot}s^{-1}$), moderate wind (5.5 $m{\cdot}s^{-1}$–8.0 $m{\cdot}s^{-1}$), hard wind (8.0 $m{\cdot}s^{-1}$–10.8 $m{\cdot}s^{-1}$), and strong wind (10.8 $m{\cdot}s^{-1}$–13.9 $m{\cdot}s^{-1}$) (Wu *et al.* 2013). The hydrological processes from June 1 to September 30 of the common-water year 2010 were determined for calculation,

during which the three water patterns were all involved. Keeping all other factors the same, the comparison calculation schemes were arranged synchronously with the wind-driven parameter closed.

RESULTS

Model calibration

The model was calibrated and validated against the field investigated sediment data at ten field investigated points in Poyang Lake during the flood season in 2010 and 2012. The calculation period for calibration was May 1, 2010 to October 31, 2010, and the period for validation was May 1, 2012 to October 31, 2012. The period of May to October was selected because the lake could undergo the three current patterns in these months. The distribution of the points is shown in Figure 1. The ten sites are Xin River west branch (No.1), Fu River estuary (No.2), Gan River south branch (No.3), Kangshan (No.4), Gan River main branch (No.5), Xiu River estuary (No.6), Benghu (No.7), Zhuxikou (No.8), Hamashi (No.9), and Hukou (No.10). The calculated area included a nearby portion of the Yangtze River, the five upstream river inlets, and Poyang Lake. In view of the surface area of the lake, the spatial resolution of the computation was set to 700 m × 700 m, giving a total of 7,533 nodes and 6,239 quadrilateral elements for the modeling area. The calculation time step of the model was dynamically adjusted according to the model grid size and water depth condition, ensuring that the CFL number (Courant–Friedrich–Levy) was less than 0.8 to meet the requirement of model stability. Approximately one-tenth of the elements were given lake bottom elevations based on field data and the remaining bathymetry was numerically calculated by the model. The measured suspended sediment concentrations and water levels of the five upstream tributaries and the downstream Yangtze River were selected as the boundary conditions. The input data of the above boundaries were supplied by Hydrology Bureau of Jiangxi Province and Bureau of Hydrology, Changjiang Water Resource Committee. The unit weight of water and suspended particles were taken as 1,000 $kg{\cdot}m^{-3}$ and 1,190 $kg{\cdot}m^{-3}$, respectively.

The Manning coefficients, wind drag coefficient, wave stress coefficient, and the dispersion coefficients of SS were used for the calibration. The Manning coefficients ranged between 0.01 and 0.035. The wave stress coefficient α is from 0.22 to 0.35. The wind drag coefficient η is between 1.288×10^{-3} and 1.445×10^{-3}. The dispersion coefficients of SS in the lake are in the scope of 0.0035–0.0052. The other parameters were obtained from previous results (Li 2008; Zhang *et al.* 2017). The vertical and the lateral diffusion coefficient of suspended sediment were taken as 1.0 $m^2{\cdot}s^{-1}$ and 0.1 $m^2{\cdot}s^{-1}$, respectively. The vertical diffusivity here was just to reflect the bottom boundary conditions. As turbulence does not play a pronounced role in the present research, the movement viscosity coefficient and eddy viscosity coefficient were taken as 1.0×10^{-6} $m^2{\cdot}s^{-1}$ and 0.5×10^{5} $cm^2{\cdot}s^{-1}$, respectively. The correction coefficient λ is a dynamic parameter that is related to wind conditions. The average wave height in the lake ranges from 0.33 m to 0.52 m, and the wave period varies between 1.75 s and 2.18 s. The critical shear stresses for erosion were obtained from laboratory results, and the fine-, medium-, and coarse-silt were characterized by the critical incipient shear stresses of 0.011 $N{\cdot}m^{-2}$, 0.017 $N{\cdot}m^{-2}$, and 0.024 $N{\cdot}m^{-2}$, respectively. As the best agreement between predicted and observed data during the calibration period was achieved by using a small time step of 1.0 s, it was adopted to obey all stability criteria and guarantee the calculation accuracy under the explicit scheme. The comparison of calculated results and field investigated data is shown in Figure 3. As the response of flow structure to current patterns varied with lake regions, i.e., marked flow changes under backflow-pattern current was observed in the north lake, and that under jacking- and gravity-pattern current in the central lake and south lake, respectively, the lake regions in Figure 3 not only show the spatial distribution but also indicate the current patterns. The mean of the absolute value of the relative error (ARE), i.e., ARE = |Calculated – measured|/measured, for the calibration and validation period was less than 20%. Considering the inevitable discrepancy between the numerical model and actual conditions, the observation error of field-investigated results, and the frequently fluctuated environmental factors in Poyang Lake, the deviation was acceptable to conduct numerical

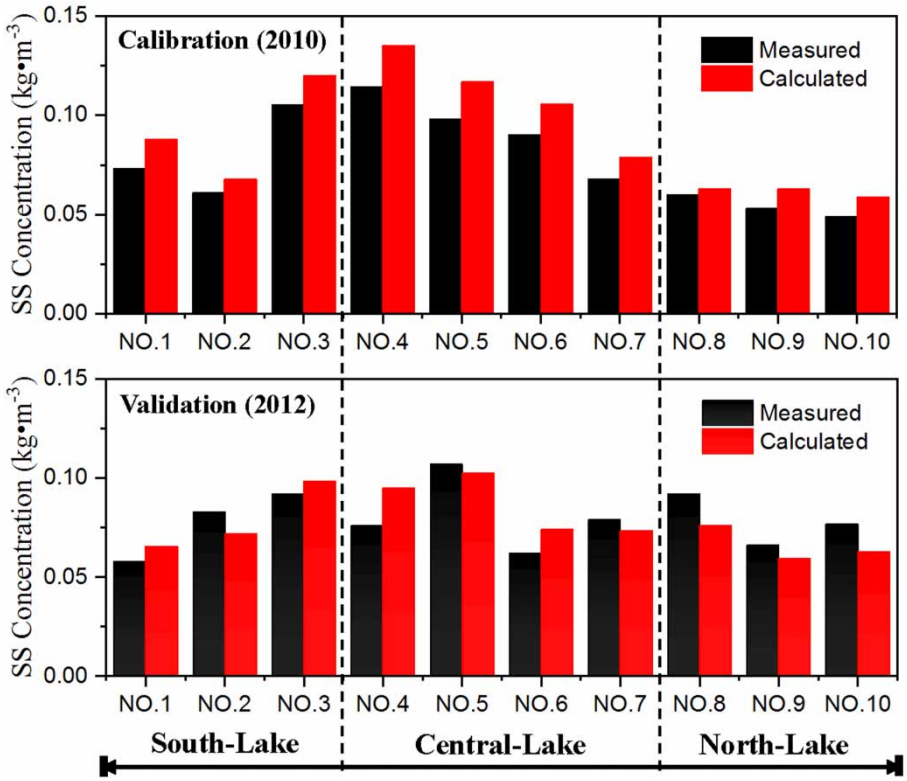

Figure 3 | Comparison between the measured values and calculated results.

simulations. The model is capable of scientifically representing the transport processes of water current and SS in Poyang Lake.

Wind's contribution to bottom shear stress

The laboratory results revealed that SS release to the overlying water was proportional to bed shear stress and the suspension is closely related to particle diameters. SS loads in the overlying water subject to weak shear stress ($<0.05\ N{\cdot}m^{-2}$) were low and just a few fine-silts were observed to preferentially suspend. After the disturbance was intensified above a critical level, the bed sediment was intensely affected and significant sediment suspension was detected. When the shear stress was approaching $0.10\ N{\cdot}m^{-2}$, the bottom sediment was observed to increasingly suspend, with the stripes becoming evidently tortuous. A fully developed suspended sediment regime was gradually established. As the bottom shear stress was increased to $0.26\ N{\cdot}m^{-2}$ the tortuous level of the stripes was significant, with the ends of the stripes gradually joining together and, swinging like a broom, which caused intense sediment suspension. SS content of the overlying water was markedly increased to 63.48%, 48.54%, and 36.41%, respectively, in the tests for fine-silt, medium-silt, and coarse-silt. Subject to the same disturbance intensity, SS contents in the overlying water of the three group tests also exhibited an evident variation with the grain size. In the present work, the suspension rate of 10% was adopted as the starting standard. Hence, the fine-, medium-, and coarse-silt were characterized by the critical incipient shear stresses of $0.011\ N{\cdot}m^{-2}$, $0.017\ N{\cdot}m^{-2}$, and $0.024\ N{\cdot}m^{-2}$, respectively (Figure 4(a)).

How wind triggers the deposited sediment to overlying water is related to the combination of water depth, wind intensity, and wind fetch (WF). Based on the lake morphology, the WFs of 10 km, 20 km, and 30 km were adopted to explore wind's contribution to the bottom shear stress of different water depths (Figure 4(b)–4(d)). It was detected that wind-generated shear stress negatively

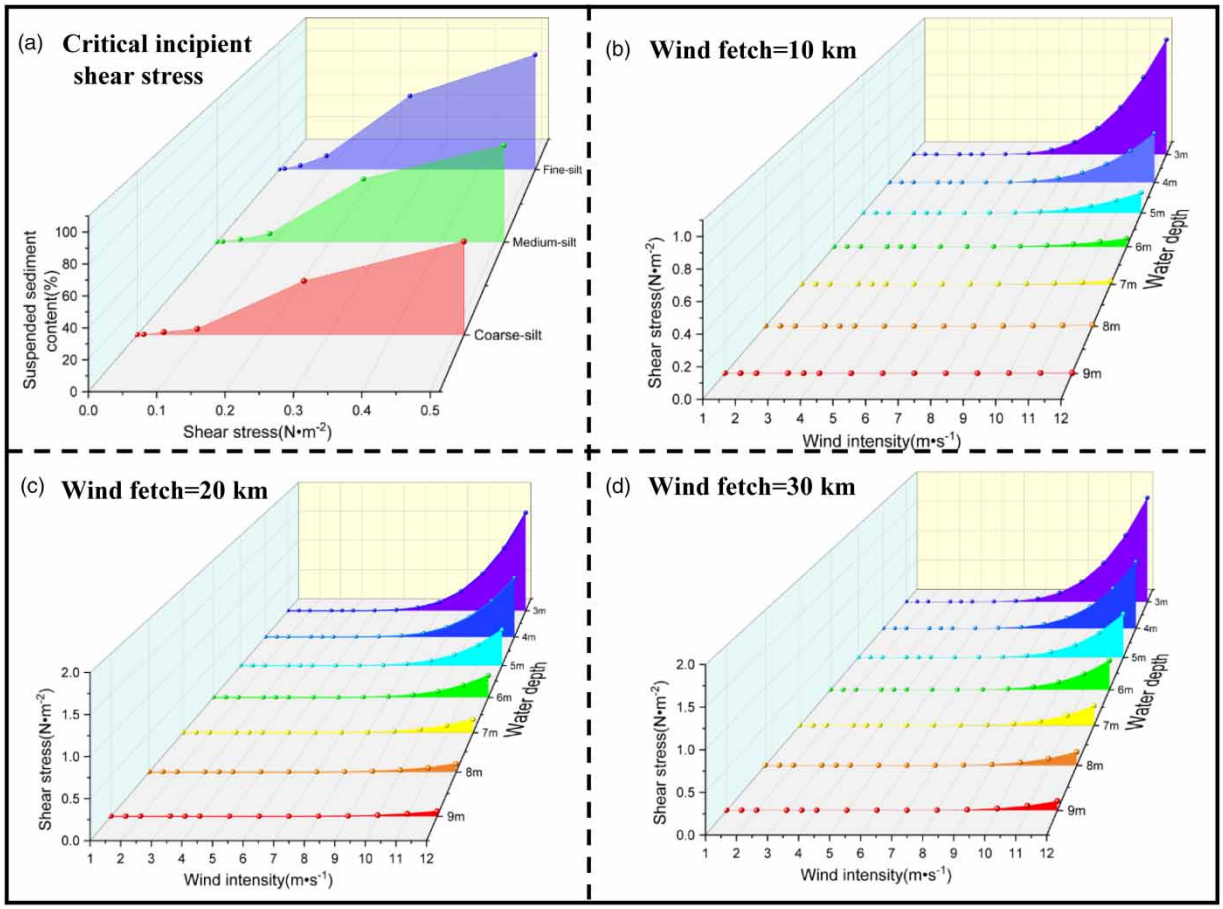

Figure 4 | (a) Relationship between shear stress and sediment suspension for fine-, medium-, and coarse-silts. (b), (c), and (d), respectively, illustrate wind's contribution to the bottom shear stress at varied water depths with the wind fetches of 10 km, 20 km, and 30 km.

correlates with water depth under the same wind fetch, i.e., in the case of $u = 6\ s{\cdot}m^{-1}$, $h = 3$ m, $WF = 10$ km, wind impact is strong enough to trigger the bottom fine-silt to suspend. However, holding u and WF the same, wind can hardly affect the bottom sediment when h was increased to 6 m. At the same water depth, wind intensity distinctly made a positive contribution to the bottom shear stress. During the event of $u = 6\ m{\cdot}s^{-1}$, $h = 4$ m, $WF = 20$ km, the bottom shear stress was just enhanced by $0.004\ N{\cdot}m^{-2}$. However, after the wind intensity rose to $7\ m{\cdot}s^{-1}$, the disturbance contribution could reach $0.019\ N{\cdot}m^{-2}$, which was capable of individually motivating the suspension of fine-silt and medium-silt. When the wind intensity went up to $8\ m{\cdot}s^{-1}$, the contributed shear stress was enhanced to $0.063\ N{\cdot}m^{-2}$, which markedly exceeded the critical starting shear stresses of fine-, medium-, and coarse-silt. WF interacts with wave height, wave length, and wave period, and thus influences the wind-driven SS dynamics. In general, if wind intensity were kept the same, wind fetch is an important factor affecting the wave height, wavelength, and wave period, which directly determines the influence of the wind on the suspension of sediments. The longer wind fetch always results in a stronger shear stress, and therefore a stronger regulation in suspended sediment distribution.

Wind impact evaluation

SS in Poyang Lake is closely related to external water volume, imported sediment concentration, hydrodynamic conditions, lake topography, and wind events. Generally, water current is the dominant factor governing the dynamics of SS. As different current patterns are characterized by

varied flow directions and intensities, wind impacts on SS transport change with current patterns. Based on the results of numerical experiments, SS distributions under the combination of different wind events and different current patterns in Poyang Lake are shown in Figure 5. The schemes are expressed by two capital letters. The first letters G, J, and B, respectively, represent the gravity-pattern, jacking-pattern, and backflow-pattern. The second letters L, G, M, H, and S, respectively, represent the light wind, gentle wind, moderate wind, hard wind, and strong wind, e.g., G-M indicates the combination of gravity-pattern current and moderate wind.

Under the gravity-pattern, water flows from the south to north. SE wind in the south lake accelerated the spreading of SS from the river inlet area to the central lake, i.e., in the case of G-S, wind of 3.61 $m{\cdot}s^{-1}$ from SE in the south lake motivated the SS from Gan-, Fu, Xin rivers to extend northwards, which enhanced the SS in NGR to 78.9 $mg{\cdot}L^{-1}$, increased by 18.5% than that without wind. However, the strong NW wind of 10.82 $m{\cdot}s^{-1}$ in the north resisted the current-driven transport from south to north, which could be evidently observed in the region south to Duchang. This resistance was generated by the combination of surface drift and Stokes drift. Under the situation of G-H, winds in

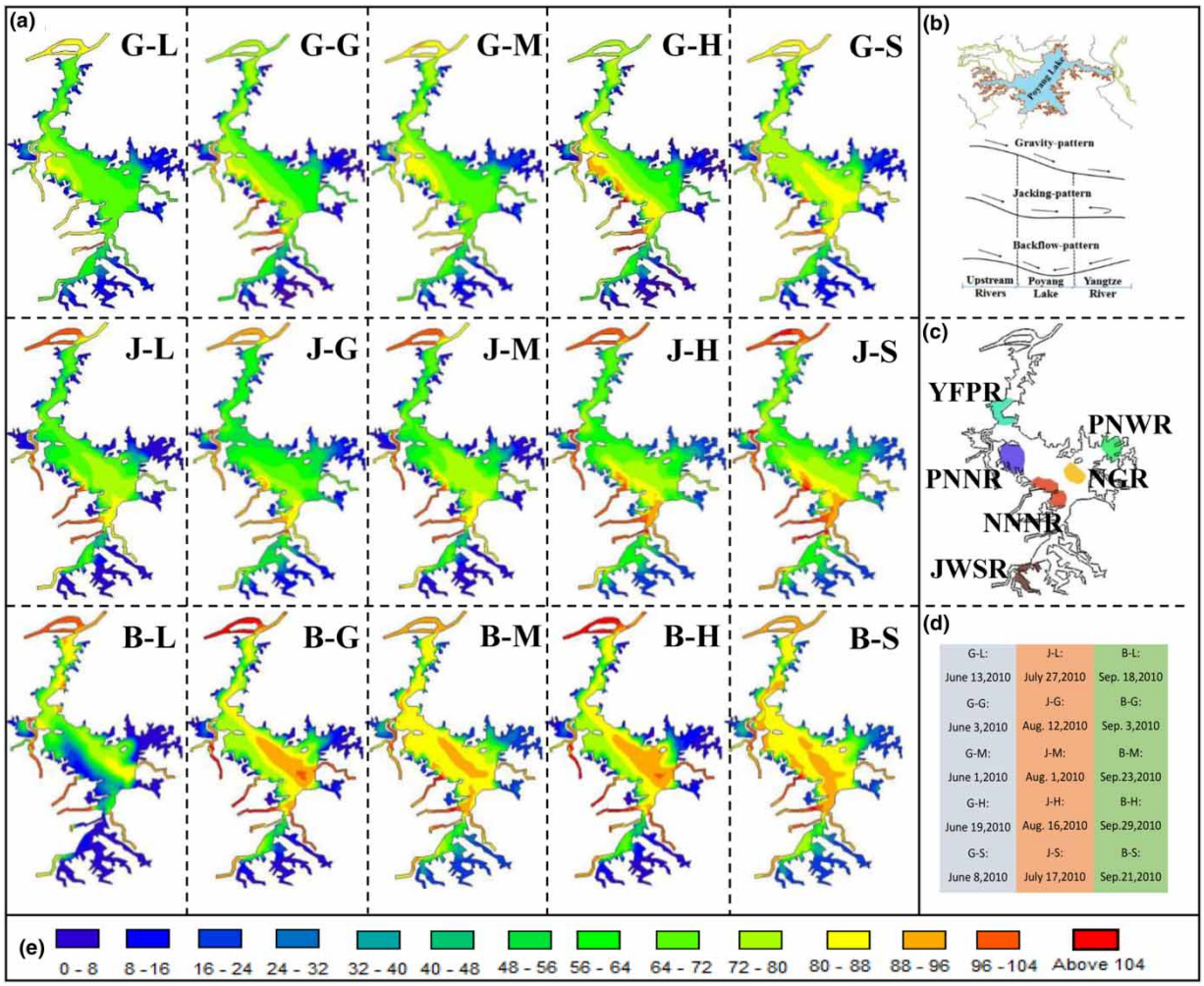

Figure 5 | (a) The SS distribution under the combination of varied currents and wind events in Poyang Lake. The two letters, respectively, indicate current pattern and wind event. (b) The flow directions under the gravity-, jacking-, and backflow-pattern current. (c) The distribution of six reserves in the computed area. (d) The dates of wind events under different current patterns. (e) The SS concentration gradient, mg/L.

the north, central, and south lake were, respectively, 9.01 $m \cdot s^{-1}$ (NE), 1.94 $m \cdot s^{-1}$ (NW), and 3.89 $m \cdot s^{-1}$ (SE). The easterly wind in north and south lake resulted in a narrowed SS diffusion zone towards the west. Hence, the SS loads in PNNR and NNNR were increased to 95 $mg \cdot L^{-1}$ and 83.1 $mg \cdot L^{-1}$, with wind contribution, respectively, being 9.10 $mg \cdot L^{-1}$ and 8.44 $mg \cdot L^{-1}$. In the case of G-M, influenced by 2.5 $m \cdot s^{-1}$ (NE) in the central lake, SS diffusion intensity from the middle branch of Gan River to the central lake was weakened. SS concentration in the inlet area was decreased by 6.13 $mg \cdot L^{-1}$ than the value without wind. In the south lake, the NW wind of 2.67 $m \cdot s^{-1}$ exhibited an inhibitory effect on SS transport from the south branch of Gan, Fu, and Xin rivers. SE wind in the north was stronger than winds in the center and south, but due to the limited wind fetch, the wind's contribution to YFPR was just 2.68 $mg \cdot L^{-1}$. In G-G mode, the south and north lake were influenced by NW winds of 2.22 $m \cdot s^{-1}$ and 3.89 $m \cdot s^{-1}$, which stemmed the SS transport driven by current. SS in PNNR was decreased to 68.7 $mg \cdot L^{-1}$. The wind direction in the central lake was consistent with water flow, whereas the weak intensity did not show any evident promotion in SS spreading northward.

Wind intensity under the G-L situation was lower, with the north and south lake influenced by SE winds of 1.11 $m \cdot s^{-1}$ and 1.39 $m \cdot s^{-1}$, and the central lake by NW wind of 1.35 $m \cdot s^{-1}$. The wind's impacts on SS dynamics were concentrated in the west lakeshore between the south branch and middle branch of Gan River. However, this contribution was not remarkable, and the fluctuation of SS in PNNR was only 0.076 $mg \cdot L^{-1}$.

During the jacking-pattern, water in the lake cannot smoothly outflow to the Yangtze River. The reduced flow disturbance weakens the sediment carrying capacity, which makes stronger the impacts of wind on SS dynamics. Besides, during the period when jacking-pattern current happens, the wind directions in different lake regions tend to be more consistent. Apart from scheme J-L, SE wind prevails in the south and north lake, and in the central lake wind shifts to the SW. In the case of J-L, the north and central lake were dominated by 1.11 $m \cdot s^{-1}$ (NE) and 1.67 $m \cdot s^{-1}$ (NE). The surface drift induced by light wind made minor contributions to SS loads in NGR and NNNR, which were, respectively, 0.86 $mg \cdot L^{-1}$ and 1.32 $mg \cdot L^{-1}$. Under the J-G scheme, SE wind in the south expanded the length of northward diffusion zone from Gan and Fu rivers, which resulted in an increase of 5.83% in PNNR and 7.05% in NNNR than the SS loads without the wind's impacts. Limited by wind fetch, wind-driven SS transport in the inlet area of Gan River south branch was lower than that in the middle branch. The increments of the SS diffusion length in the two inlet areas were, respectively, 0.83 km and 3.77 km. In the central lake, SW wind tended to push the SS diffusion zone to the central mainstream area. However, as a result of the low wind intensity, this contribution to SS load was not marked, with the mean value being 1.57 $mg \cdot L^{-1}$. In the situation of J-M, SE wind in the south significantly increased the SS diffusion range to the central lake from Gan, Fu, and Xin rivers. The mean SS concentration in the central lake was increased to 78.9 $mg \cdot L^{-1}$, 12.6% higher than that without wind. With the SW wind prevailing, SS transported by the middle branch of Gan River made a certain contribution to SS load in the central lake. SS in the eastern area of NNNR was detected with an increase of 2.69 $mg \cdot L^{-1}$. In schemes of J-H and J-S, the south wind not only further promoted SS transport from the south to the central, but triggered the suspension of surface sediments in lakeshore areas. Wind showed a much stronger regulation in SS loads of PNNR, NGR, and NNNR with the mean contributions of 12.5%, 13.8%, and 15.4%, respectively. Wind direction in the north also became southerly, which promoted the northward transport of SS from Xiu River and the north branch of Gan River. SS load in YFPR was approximately increased by 3.7 $mg \cdot L^{-1}$.

For the backflow-pattern, the northern narrow 'throat' area linking the main lake and Yangtze River is characterized by strong water currents. Sediments from the Yangtze River are transported from the north to south, feeding the SS load in the north lake. Under the B-L scheme, NE wind in the north generated a minor contribution of 0.95 $mg \cdot L^{-1}$ to SS in YFPR. In the central lake, SE wind, to some extent, diminished the inverted sediment, and SS in PNNR was decreased by 0.73 $mg \cdot L^{-1}$ than that without wind. In the case of B-G, NW wind in the south drove sediments from the middle, north branch of Gan River and Fu River to move towards the eastern lake, thus resulting in a decrease of 8.35% in NNNR sediment concentration. The response of SS in the central lake to SE wind was featured

by an apparent concentration gradient. SS loads in NGR with and without wind were, respectively, 85.9 mg·L^{-1} and 78.7 mg·L^{-1}. SE wind in the north made stronger the inhibition on the southerly SS transport. SS spread from YFPR to the main lake was reduced, and the mean concentration was 88.6 mg·L^{-1}, approximately 6.7 mg·L^{-1} higher than that without wind. In the situation of B-M, SE wind in the north was enhanced to 7.78 m·s^{-1} that effectively obstructed the sediment input from the Yangtze River in the narrow 'throat' area where the SS load was increased by 11.56%. In the lakeshore area near Xingzi, a SS belt, 2.76 km in length and 0.75 km in width, was observed with the mean concentration of 95.3 mg·L^{-1}. Since SW wind in the south repressed the NW wind in the central lake, the SS gradient band near NGR was constricted. As NW wind prevailed in the south lake under the B-H scheme, SS from the middle and south branch of Gan River was driven to the southeast, and SS in NNNR fell to 80.5 mg·L^{-1}. Attributed to the additive effects of wind-induced sediment suspension and inverted transport from the Yangtze River, the mean SS concentration in the middle-east lake rose to 87.2 mg·L^{-1}. Under the scheme B-S, the whole lake was influenced by SE wind. The intensity in the north could reach 11.11 m·s^{-1} that further blocked the inverted sediment in the narrow pathway, leading to the sediment increase of 19.6% in YFPR. In the central lake, PNNR and NNNR were also observed to rise in SS loads, which were, respectively, 12.6 mg·L^{-1} and 17.5 mg·L^{-1}. Wind drove the sediment band near the mainstream to deflect westwards, thus leading to a decline of 8.27% in SS load of NGR.

DISCUSSION

In general, wind impacts on SS transport increase with rising wind intensities. Light and gentle winds can hardly trigger the deposited sediment suspension to overlying water, but the surface drifts induced by them are still able to reorder the spatial distribution of SS in the lake. The regulations of moderate, hard, and strong winds on lake currents are more remarkable, and the influence on SS dynamics was enhanced. However, how winds affect the SS distribution is closely related to their direction. When wind direction coincides with current, SS under the combined effect of wind and currents showed a much stronger relationship to the background concentration of the area in the upwind direction than currents alone. This relationship can be attributed to the enhanced surface drift and the Stokes drift induced by waves at different water depth. However, when wind shifts to the opposite direction of currents, SS transport should face resistance, the strength of which is determined by wind intensity. Winds not only affect the horizontal transport of SS, but also regulate the vertical dynamics. In the event of moderate, hard, and strong wind, when the duration and wind fetch are met, the stronger bottom shear stress may trigger sediment suspension to feed the loads in overlying water, especially in the eastern and western lakeshore.

Wind's impacts on SS dynamics also have a relationship with lake morphologies. The central lake is characterized by the most instable wind direction, with the frequencies of NW, SE, NE, and SW being, respectively, 20.2%, 33.3%, 26.7%, and 19.8%, and the lowest mean wind speed of 3.44 m·s^{-1}, but it has a broad water surface, which permits the formation of continuous waves. Hence, the wind-induced impacts on SS dynamic is most notable in the central lake, and can be generalized into the following aspects: (1) accelerating the sediment transport from southern rivers to the north; (2) repressing the backflow sediment from the Yangtze River; and (3) reordering the SS loads in the east and west lake beside the mainstream. The south and north lake both have prevailing SE wind, with the frequencies, respectively, being 56.3% and 66.7%, and the mean wind speeds are higher than those in the central lake, which are 5.59 m·s^{-1} and 4.19 m·s^{-1}, respectively. However, SS in the south and north lake generally undergoes a lower wind impact than that in the central lake. The fluctuation in SS concentration induced by wind in the south and north lake approximately ranges from -6.59 mg·L^{-1} to $+10.36$ mg·L^{-1}, while that in the central lake is between -10.05 mg·L^{1} and $+20.17$ mg·L^{-1}. The different influence degrees are probably due to the following two reasons. First, the surfaces of the south and north lake are narrower than that of the central lake and it is harder for waves to be generated under the same wind speed for the limited wind fetch. Second, the section morphologies in the south and north lake enhanced the flow velocity, which weakens the wind impacts.

In the six ecological reserves, NGR (National Germplasm Reserve), YFPR (Yangtze Finless Porpoise Reserve), PNNR (Poyang National Nature Reserve), NNNR (Nanjishan National Nature Reserve), PNWR (Poyang National Wetland Reserve), and JWSR (Jiangxi Whitebait Spawning Reserve), wind influences on SS dynamics are observed with marked variation (Figure 6). PNWR and JWSR are located in the marginal area where the sediment carrying capacity is lower and the wind fetch is limited. When the prevalent wind in the central lake becomes more westerly, sediments in the main lake could make a minor contribution towards PNWR. The increase of SS in JWSR was more easily found after the wind in the south lake shifted to a north direction, but the mean contributions of wind were only 4.12% and 4.08%, respectively. SS loads in the two reserves show no obvious departure from those without wind. SS concentrations in YFPR, PNNR, NNNR, and NGR are characterized by more remarkable wind impacts, and the means of 10.3%, 12.7%, 13.2%, and 9.3% were enhanced by wind, respectively. Nevertheless, the influencing weights in different reserves had close relationships with current patterns, wind speeds, and wind directions. For example, when the prevalent south wind in the central lake repressed sediments from the Yangtze River, the regulation of wind in YFPR was distinguished at the highest level. The degrees of wind impacts in PNNR, NNNR, and NGR were enhanced with rising wind speeds, especially in the events of high and strong winds. When wind acts as a hindrance to SS transport, its resistance ability is closely related to current intensity, i.e., in the central lake, the flow currents are reduced by the board water surface, and the mean resistance rate in PNNR, NNNR, and NGR could reach 6.2%. However, in YFPR where the flow current is stronger, the mean resistance rate was just 2.3%.

These results could yield insight into wind impacts on SS dynamics in Poyang Lake. However, there are several

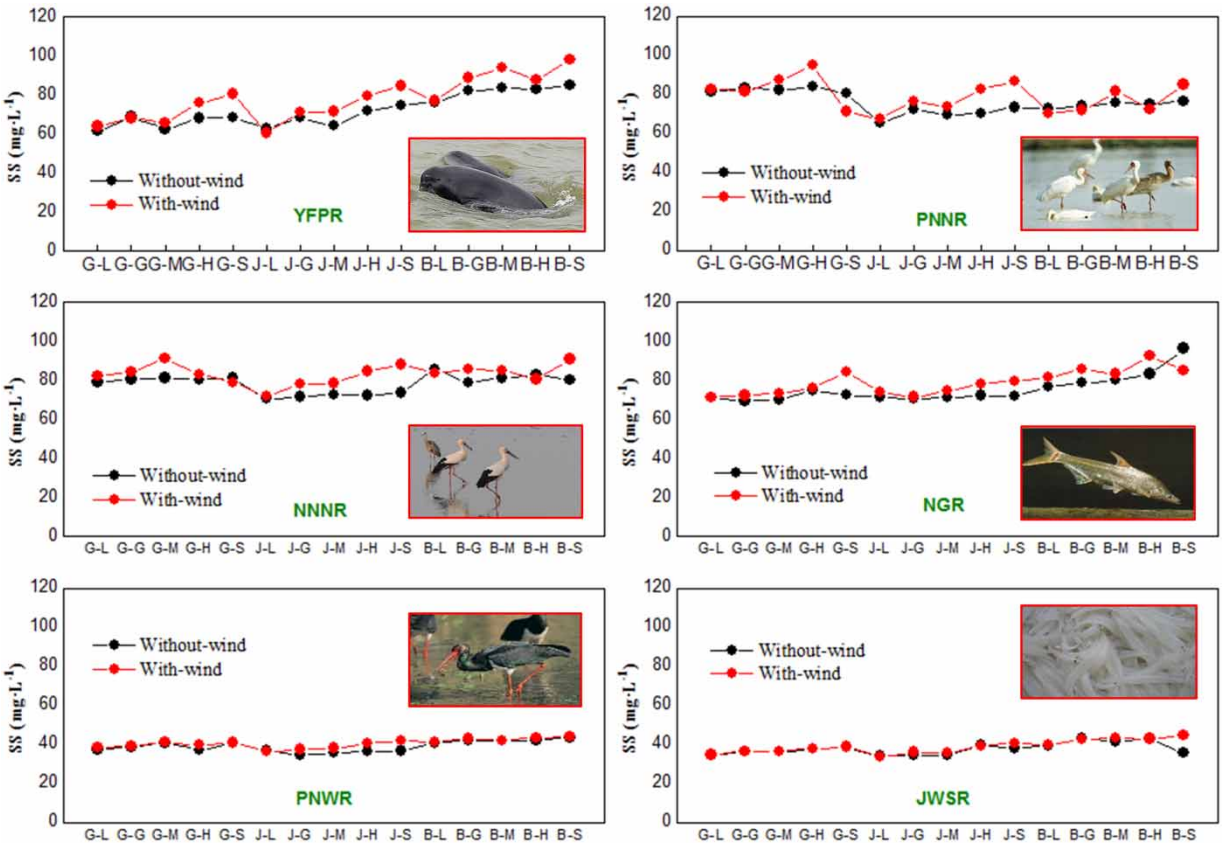

Figure 6 | Comparison between the SS concentrations with and without wind in the reserves of Poyang Lake.

uncertainties that may need further investigation. First, in the present work, the interactions of sediments with some ecological processes were not considered, i.e., plant blocking, biological consumption, and bioaccumulation. Simplification of these interactions indeed set up a barrier to simulate the field actual SS transport, but it will not affect the general trend of the dynamics in the whole lake. Second, a lack of monitored data meant the model suffered from not accurately incorporating the sediment input of some small boundary rivers, which was recognized as a constant for the present work. Third, the model we established here was a depth-averaged one, and the vertical SS transport was simplified by the parameters of deposition and suspension.

CONCLUSIONS

Combining field data, laboratory experiment, and numerical simulation, we shed light on the wind impacts on SS dynamic in Poyang Lake. Wind impacts increase with rising wind speeds. They not only affect the horizontal SS transport, but also regulate the vertical dynamics. When the wind direction coincides with current direction, SS under the combined effect of wind and current showed a much stronger correlation with the background concentration in the upstream area than the situation without wind. High-speed wind can enhance the horizontal transport by both surface drift and Stokes drift at different water depths, and trigger sediment suspension to feed the loads in overlying water. Wind impacts on SS dynamics also have to do with the lake morphology. The central lake is characterized by a large open water area, which permits the formation of continuous waves, leading to the highest degree of variation in SS concentration. However, due to the limited wind fetch and stronger flow currents, SS in the south and north parts of the lake generally observes a much weak impact from the wind. Attributed to the geographical location, SS loads in PNWR and JWSR show no obvious departure from those without wind. However, the YFPR, PNNR, NNNR, and NGR experience notable wind impacts. The paper provides technical support for policy makers who try to understand the variation of SS in Poyang Lake and is also relevant regarding the protection of the ecological balance in other large inland freshwater lakes.

ACKNOWLEDGEMENTS

This work was supported by the National Natural Science Foundation of China (No.51779075), Water conservancy science and technology project of Jiangxi Province (KT201623), the Major Science and Technology Program for Water Pollution Control and Treatment of China (2017ZX07203002–01), Qing Lan Project, and A Project Funded by the Priority Academic Program Development of Jiangsu Higher Education Institutions.

REFERENCES

Cao, J. H., Liu, X. M., Li, G. P. & Zou, H. B. 2015 Analysis of the phenomenon of lake-land breeze in Poyang Lake area. *Plateau Meteorology* **34** (2), 426–435. (in Chinese, with English Abstr.).

Carlin, J. A., Lee, G., Dellapenna, T. M. & Laverty, P. 2016 Sediment resuspension by wind, waves, and currents during meteorological frontal passages in a micro-tidal lagoon. *Estuarine, Coastal and Shelf Science* **172**, 24–33.

Chao, X. B., Jia, Y. F., Douglas, F., Wang, S. Y. & Cooper, C. M. 2008 Three-dimensional numerical modeling of cohesive sediment transport and wind wave impact in a shallow oxbow lake. *Advances in Water Resources* **31**, 1004–1014.

Cheng, C. M., Wei, Y. C., Xu, J. J. & Yuan, Z. J. 2013 Remote sensing estimation of Chlorophyll a and suspended sediment concentration in turbid water based on spectral separation. *Optik-International Journal for Light and Electron Optics* **124** (24), 6815–6819.

Choi, S. & Lee, J. 2015 Assessment of total sediment load in rivers using lateral distribution method. *Journal of Hydro-Environment Research* **9**, 381–387.

Constantin, A. 2006 The trajectories of particles in Stokes waves. *Inventiones Mathematicae* **166**, 523–535.

Constantine, J. A., Dunne, T., Ahmed, A., Legleiter, C. & Lazarus, E. D. 2014 Sediment supply as a driver of river meandering and floodplain evolution in the Amazon Basin. *Nature Geoscience* **7**, 899–903.

Cui, L. J., Qiu, Y., Fei, T., Liu, Y. L. & Wu, G. F. 2013 Using remotely sensed suspended sediment concentration variation to improve management of Poyang Lake, China. *Lake and Reservoir Management* **29**, 47–60.

Dag, M. 2015 Stokes drift estimation based on long-term variation of wave conditions. *Journal of Engineering for the Maritime Environment* **229** (2), 141–146.

Day, J. W., Britsch, L. D., Hawes, S. R., Shaffer, G. P., Reed, D. J. & Cahoon, D. 2000 Pattern and process of land loss in the Mississippi Delta: a spatial and temporal analysis of wetland habitat change. *Estuaries* **23**, 425–438.

Draut, A. E., Kineke, G. C., Huh, O. K., Grymes III., J. M., Westphal, K. A. & Moeller, C. C. 2005 Coastal mudflat accretion under energetic conditions, Louisiana chenier-plain coast, USA. *Marine Geology* **214**, 27–47.

Edmonds, D. A. & Slingerland, R. L. 2010 Significant effect of sediment cohesion on delta morphology. *Nature Geoscience* **3**, 105–109.

Feng, L., Hu, C., Chen, X. L. & Zhao, X. 2013 Dramatic inundation changes of China's two largest freshwater lakes linked to the Three Gorges Dam. *Environmental Science and Technology* **47**, 9628–9634.

Gao, J. H., Jia, J. J., Kettner, A. J., Xing, F., Wang, Y. P., Xu, X. N., Yang, Y., Zou, X. Q., Gao, S. & Qi, S. H. 2014 Changes in water and sediment exchange between the Changjiang River and Poyang Lake under natural and anthropogenic conditions, China. *Science of the Total Environment* **481**, 542–553.

Guo, H., Hu, Q. & Jiang, T. 2008 Annual and seasonal streamflow responses to climate and land-cover changes in the Poyang Lake basin, China. *Journal of Hydrology* **355**, 106–122.

Han, X. X., Chen, X. L. & Feng, L. 2015 Four decades of winter wetland changes in Poyang Lake based on Landsat observation between 1973 and 2013. *Remote Sensing of Environment* **156**, 426–437.

Hawley, N., Harris, C. K., Lesht, B. M. & Clites, A. H. 2009 Sensitivity of a sediment transport model for Lake Michigan. *Journal of Great Lakes Research* **35** (4), 560–576.

Horowitz, A. J. 2008 Determining annual suspended sediment and sediment-associated trace element and nutrient fluxes. *Science of the Total Environment* **400** (1–3), 315–343.

Hossain, S., Eyre, B. D. & McKee, L. J. 2004 Impacts of dredging on dry season suspended sediment concentration in the Brisbane River estuary, Queensland, Australia. *Estuarine, Coastal and Shelf Science* **61** (3), 539–545.

Jan, E. W. 1982 Steady wind- and wave-induced currents in the open ocean. *Journal of Physical Oceanography* **13**, 524–530.

Jane, M. M., John, B. A. & Robert, B. D. 1987 Suspended sediment transport, sedimentation, and resuspension in Lake Houston, Texas: Implications for water quality. *Environmental Geology and Water Science* **10** (3), 175–186.

Ji, Y., Xu, X. F., Wan, J. B. & Hu, S. T. 2012 Research on simulation of diversion flood routing for Kangshang flood storage in Poyang Lake region. *Procedia Engineering* **28**, 740–743.

Lei, S., Zhang, X. P. & Xu, X. F. 2010 Remote sensing based analysis and dynamic monitoring on area and storage of Poyang Lake. *Water Res. Hydro. Eng.* **41**, 83–90. (in Chinese with English Abstr.).

Li, S. C. 2008 *Research on Statistical Characteristics and Calculation Methods of Wind-Wave of Poyang-Lake*. *Dissertation*, Changsha University of Science and Technology, Changsha.

Liu, Q. & Rossiter, D. G. 2008 Estimation on suspended sedimentation concentration of Poyang Lake using MODIS and hyperspectral data. *Remote Sensing Technology Applications* **23** (1), 7–11.

Lu, M., Zeng, D. C., Liao, Y. & Tong, B. 2012 Distribution and characterization of organochlorine pest-icides and polycyclic aromatic hydrocarbons in surface sediment from Poyang Lake, China. *Science of the Total Environment* **433**, 491–497.

Mekete, D., Verhoest, N. E. C., Pauwels, V. R. N., Enyew, A., Jozef, D., Jean, P. & Jan, N. 2015 Water balance of a lake with floodplain buffering: Lake Tana, Blue Nile Basin, Ethiopia. *Journal of Hydrology* **522**, 174–186.

Pang, Q. X., Bai, Y. C., Yang, H., Zhang, R. B. & Jia, Z. B. 2012 Critical stress profile for incipient sediment motion on muddy shoals. *Advances in Water Science* **23** (2), 249–255. (in Chinese with English Abstr.).

Perez, B., Day, J., Rouse, L., Shaw, R. & Wang, M. 2000 Influence of Atchafalaya River discharge and winter frontal passage on suspended sediment concentration and flux in Fourleague Bay, Louisiana. *Estuarine Coastal and Shelf Science* **50**, 271–290.

Periáñez, R. 2009 Environmental modelling in the Gulf of Cadiz: heavy metal distributions in water and sediments. *Science of the Total Environment* **407**, 3392–3406.

Poff, N. L., Allan, J. D. & Bain, M. B. 1997 The natural flow regime. A paradigm for river conservation and restoration. *BioScience* **47**, 769–784.

Pu, J. H. 2015 Turbulence modelling of shallow water flows using Kolmogorov approach. *Computers and Fluids* **115**, 66–74.

Pu, J. H. 2019 Turbulent rectangular compound open channel flow study using multi-zonal approach. *Environmental Fluid Mechanics* **19** (3), 785–800.

Pu, J. H., Cheng, N. S. & Tan, S. K. 2012 Source term treatment of SWEs using the surface gradient upwind method. *Journal of Hydraulic Research* **50** (2), 145–153.

Qiu, H. M., Geng, J. J., Ren, H. Q. & Xu, Z. Y. 2016 Phosphite flux at the sediment-water interface in northern Lake Taihu. *Science of the Total Environment* **543**, 67–74.

Ran, Q. H., Tong, J., Shao, S. D., Fu, X. D. & Xu, Y. P. 2015 Incompressible SPH scour model for movable bed dam break flows. *Advances in Water Resources* **82**, 39–50.

Sheng, Y. P. & Lick, W. 1979 The transport and resuspension of sediments in a shallow lake. *Journal of Geophysical Research* **84** (NC4), 1809–1826.

Snorri, P. K., Sigurdur, L. H. & Eric, M. M. 2004 Lake circulation and sediment transport in Lake Myvatn. *Aquatic Ecology* **38**, 145–162.

Stokes, G. G. 1847 On the theory of oscillatory waves. *Transactions of the Cambridge Philosophical Society* **8**, 441–455.

Su, H. L., Lin, Y. H., Li, D. Q. & Qian, F. W. 2000 Status of Chinese cranes and their conservation strategies. *Chinese Biodiversity* **8** (2), 180–191.

Thomas, T. G. & Takhar, H. S. 1992 Turbulent mass transport and attenuation in Stokes waves. *Applied Scientific Research* **49**, 1–29.

Volpe, V., Silvestri, S. & Marani, M. 2011 Remote sensing retrieval of suspended sediment concentration in shallow waters. *Remote Sensing of the Environment* **115** (1), 44–54.

Wang, J., Zhou, J. J. & Zhang, C. K. 2014 Experimental study on velocity distribution of two-direction rotating annular flume. *Journal of Sediment Research* **5**, 32–37.

Wang, H., Zhang, Z. Z., Song, D. P., Zhou, Y. Y. & Liu, X. D. 2015 Water and sediment transport mechanisms in a large river-connected lake. *Water and Environment Journal* **29** (3), 391–401.

Wang, H., Zhang, Z. Z., Liang, D. F., Du, H. B., Pang, Y., Hu, K. M. & Wang, J. J. 2016 Separation of wind's influence on harmful cyanobacterial blooms. *Water Research* **98**, 280–292.

Wang, H., Zhao, Y., Liang, D., Deng, Y. & Pang, Y. 2017 30+ year evolution of Cu in the surface sediment of Lake Poyang, China. *Chemosphere* **168**, 1604–1612.

Westall, F. 2005 Life on the early earth: a sedimentary view. *Science* **308**, 366–367.

Wu, G. F., Leeuw, J. D., Skidmore, A. K., Prins, H. T. & Liu, Y. L. 2007 Concurrent monitoring of vessels and water turbidity enhances the strength of evidence in remotely sensed dredging impact assessment. *Water Research* **41**, 3271–3280.

Wu, Q., Nie, Q. S., Zhou, R. W. & Xu, W. M. 2013 Analysis of wind energy resources reserves and characteristics in mountain area of Jiangxi Province. *Journal of Natural Resources* **28** (9), 1605–1614. (in Chinese with English Abstr.).

Xiao, H., Cao, Z. D., Zhao, Q. & Han, H. S. 2009 Experimental study on incipient motion of coherent silt under wave and flow action. *Journal of Sediment Research* **3**, 75–80.

Xiong, D. G. 1990 Investigation on silt source of Poyang Lake and recent sediment regularity of the lake basin. *Oceanologia et Limnologia Sinica* **21** (4), 374–385.

Yang, M. Q. & Wang, G. L. 1995 The incipient motion formulas for cohesive fine sediments. *Journal of Basic Science and Engineering* **3** (1), 99–109.

Yarnell, S. M., Mount, J. F. & Larsen, E. W. 2006 The influence of relative sediment supply on riverine habitat heterogeneity. *Geomorphology* **80**, 310–324.

Yin, S., Wu, Y. H., Xu, W., Li, Y. Y., Shen, Z. Y. & Feng, C. H. 2016 Contribution of the upper river, the estuarine region, and the adjacent sea to the heavy metal pollution in the Yangtze Estuary. *Chemosphere* **155**, 564–572.

You, H. L., Xu, L. G., Liu, G. L., Wang, X. L., Wu, Y. M. & Jiang, J. H. 2015 Effects of inter-annual water level fluctuations on vegetation evolution in typical wetlands of Poyang Lake, China. *Wetlands* **35**, 931–943.

Zhang, L. L., Yin, J. X., Jiang, Y. Z. & Wang, H. 2012 Relationship between the hydrological conditions and the distribution of vegetation communities within the Poyang Lake National Nature Reserve, China. *Ecological Informatics* **11**, 65–75.

Zhang, S. Y., Liu, Y. X., Yang, Y. H., Sun, C. & Li, F. X. 2016 Erosion and deposition within Poyang Lake: evidence from a decade of satellite data. *Journal of Great Lakes Research* **42** (2), 364–374.

Zhang, P., Chen, X. L., Lu, J. Z., Zhang, W. & Xiao, X. W. 2017 Suspended sediment transport modeling of Poyang Lake in the wet season based on remote sensing data. *Geomatics and Information Science of Wuhan University* **42** (3), 369–376.

Zhao, X., Wang, D. & Turvey, S. T. 2012 Distribution patterns of Yangtze finless porpoises in the Yangtze River: implications for reserve management. *Animal Conservation* **16** (5), 500–518.

Zhong, D. Y., Wang, G. Q. & Wu, B. S. 2014 Drift velocity of suspended sediment in turbulent open channel flows. *Journal of Hydraulic Engineering* **140** (1), 35–47.

First received 11 September 2019; accepted in revised form 7 February 2020. Available online 9 July 2020